

## Carbene-Functionalized Ruthenium Nanoparticles

Wei Chen, James R. Davies, Debraj Ghosh, Moony C. Tong, Joseph P. Konopelski, and Shaowei Chen\*

Department of Chemistry and Biochemistry, University of California, 1156 High Street, Santa Cruz, California 95064

Received July 11, 2006. Revised Manuscript Received August 15, 2006

Stable ruthenium nanoparticles were synthesized by protecting the particles with diazo molecules that reacted readily with the ruthenium surface forming Ru=C carbene bonds, as manifested in Fourier transform infrared and  $^1\text{H}$  NMR measurements. The resulting particles, with the core diameter averaged at  $2.12 \pm 0.72$  nm as determined by transmission electron microscopic measurements, showed a Mie scattering profile in optical absorption measurements. In electrochemical studies, the particles exhibited interesting quantized charging characteristics, similar to those observed with alkanethiolate-protected gold (AuSR) nanoparticles. In addition, a proof-of-concept experiment was carried out to demonstrate that metathesis reactions on ruthenium surfaces might be exploited for the chemical functionalization of the particles through efficient surface place exchange reactions.  $^1\text{H}$  NMR spectroscopy was used to monitor the reaction kinetics which exhibited a rate constant twice that observed with AuSR particles with another thiol ligand.

### Introduction

Metal and semiconductor nanoparticles have stimulated intensive basic and technological research because of their unique chemical and physical properties that differ vastly from those of bulk materials and molecular species.<sup>1</sup> Such nanoscale particles show great potential as the novel functional structural elements in very diverse applications such as nanoelectronic devices,<sup>2,3</sup> multifunctional catalysts,<sup>4,5</sup> chemical sensors,<sup>6,7</sup> data storage,<sup>8,9</sup> biological labeling,<sup>10</sup> and so forth. Of these, monolayer-protected nanoparticles represent a unique class of nanomaterials.<sup>11</sup> For instance, the particle chemical/physical properties can be readily manipulated by surface place exchange reactions where multiple functional moieties can be incorporated into the particle protecting layer and serve as a starting point for more complicated chemical decorations.<sup>12–16</sup> Consequently the particles behave as multifunctional reagents. Such unique

properties have been demonstrated extensively by alkanethiolate-protected gold nanoparticles which undergo exchange reactions with other thiol derivatives by taking advantage of the strong affinity of thiols to gold surfaces.<sup>14–18</sup> The resulting surface composition can then be quantitatively evaluated by using a variety of spectroscopic techniques.

In addition, the particles exhibit molecular-capacitor characteristics thanks to the low-dielectric nature of the protecting layer and the nanosized dimension of the metal core. This is first exemplified by alkanethiolate-protected gold (AuSR) nanoparticles.<sup>19,20</sup> In electrochemical measurements, multiple well-defined voltammetric peaks can be observed which are ascribed to the discrete charging to the particle (sub)attofarad molecular capacitance, the so-called nanoparticle quantized charging. Recently, such discrete charging behaviors have also been observed with several other metal particles, such as Cu,<sup>21</sup> Pd,<sup>22–24</sup> and Ag.<sup>25</sup>

\* To whom all correspondence should be addressed. E-mail: schen@chemistry.ucsc.edu.

- (1) Schmid, G. *Chem. Rev.* **1992**, *92*, 1709–1727.
- (2) Andres, R. P.; Bielefeld, J. D.; Henderson, J. I.; Janes, D. B.; Kolagunta, V. R.; Kubiak, C. P.; Mahoney, W. J.; Osifchin, R. G. *Science* **1996**, *273*, 1690–1693.
- (3) Berven, C. A.; Clarke, L.; Mooster, J. L.; Wybourne, M. N.; Hutchison, J. E. *Adv. Mater.* **2001**, *13*, 109–113.
- (4) Mohr, C.; Hofmeister, H.; Radnik, J.; Claus, P. *J. Am. Chem. Soc.* **2003**, *125*, 1905–1911.
- (5) Lewis, L. N. *Chem. Rev.* **1993**, *93*, 2693–2730.
- (6) Emery, S. R.; Haskins, W. E.; Nie, S. M. *J. Am. Chem. Soc.* **1998**, *120*, 8009–8010.
- (7) Zayats, M.; Kharitonov, A. B.; Pogorelova, S. P.; Lioubashevski, O.; Katz, E.; Willner, I. *J. Am. Chem. Soc.* **2003**, *125*, 16006–16014.
- (8) Sun, S. H.; Murray, C. B.; Weller, D.; Folks, L.; Moser, A. *Science* **2000**, *287*, 1989–1992.
- (9) Sun, T.; Seff, K. *Chem. Rev.* **1994**, *94*, 857–870.
- (10) Hainfeld, J. F. *Science* **1987**, *236*, 450–453.
- (11) Brust, M.; Walker, M.; Bethell, D.; Schiffrin, D. J.; Whyman, R. *J. Chem. Soc., Chem. Commun.* **1994**, 801–802.
- (12) Templeton, A. C.; Wuelfing, M. P.; Murray, R. W. *Acc. Chem. Res.* **2000**, *33*, 27–36.

- (13) Warner, M. G.; Reed, S. M.; Hutchison, J. E. *Chem. Mater.* **2000**, *12*, 3316–3320.
- (14) Shenhar, R.; Rotello, V. M. *Acc. Chem. Res.* **2003**, *36*, 549–561.
- (15) Wellsted, H.; Sitsen, E.; Carageorghopol, A.; Chechik, V. *Anal. Chem.* **2004**, *76*, 2010–2016.
- (16) Rothrock, A. R.; Donkers, R. L.; Schoenfish, M. H. *J. Am. Chem. Soc.* **2005**, *127*, 9362–9363.
- (17) Ingram, R. S.; Hostetler, M. J.; Murray, R. W. *J. Am. Chem. Soc.* **1997**, *119*, 9175–9178.
- (18) Templeton, A. C.; Cliffel, D. E.; Murray, R. W. *J. Am. Chem. Soc.* **1999**, *121*, 7081–7089.
- (19) Ingram, R. S.; Hostetler, M. J.; Murray, R. W.; Schaaff, T. G.; Khoury, J. T.; Whetten, R. L.; Bigioni, T. P.; Guthrie, D. K.; First, P. N. *J. Am. Chem. Soc.* **1997**, *119*, 9279–9280.
- (20) Chen, S. W.; Ingram, R. S.; Hostetler, M. J.; Pietron, J. J.; Murray, R. W.; Schaaff, T. G.; Khoury, J. T.; Alvarez, M. M.; Whetten, R. L. *Science* **1998**, *280*, 2098–2101.
- (21) Chen, S. W.; Sommers, J. M. *J. Phys. Chem. B* **2001**, *105*, 8816–8820.
- (22) Chen, S. W.; Huang, K.; Stearns, J. A. *Chem. Mater.* **2000**, *12*, 540–547.
- (23) Kim, Y. G.; Garcia-Martinez, J. C.; Crooks, R. M. *Langmuir* **2005**, *21*, 5485–5491.

However, quantized charging with other particles remains elusive, most probably because of the limitation of feasible synthetic routes for the preparation of nanometer-sized, stable, and monodisperse particle molecules.<sup>26</sup>

In this article, we report the synthesis of monodisperse ruthenium nanoparticles which are stabilized by virtue of the strong affinity of diazo derivatives to fresh ruthenium surfaces with the formation of Ru=C  $\pi$  bonds. The resulting particles exhibit interesting metathesis-based exchange reaction properties with vinyl-terminated molecules, of which the reaction dynamics and extent can be accurately monitored by proton NMR spectrometry. This is motivated by a recent report by Tulevski et al.<sup>27</sup> where they found that a freshly prepared Ru thin film reacted at room temperature with diazomethane to form stable carbene monolayers on the ruthenium surface by a ruthenium-carbon double bond. Such metal-carbon multiple bonds provide chemically reactive sites for in situ molecular wire growth.

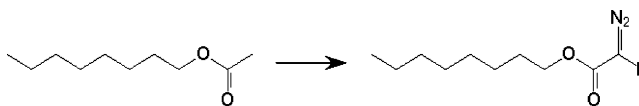
In addition, in electrochemical measurements, these ruthenium nanoparticles exhibit well-defined voltammetric features that can be attributed to the quantized charging of the particle capacitance. It should be noted that ruthenium is well-known for its catalytic activities, especially in Ru-Pt alloys that have been found to be one of the most effective electrocatalysts used in direct methanol fuel cells.<sup>28,29</sup> Thus an understanding of the charge-transfer properties of nano-sized Ru particles may help provide a fundamental insight into the mechanistic role of ruthenium in the fuel cell reactions.

## Experimental Section

**Chemicals.** Ruthenium chloride (RuCl<sub>3</sub>, 99+%, ACROS), 1,2-propanediol (ACROS), sodium acetate trihydrate (NaAc·3H<sub>2</sub>O, MC&B), 11-bromo-1-undecene (95%, Sigma-Aldrich), 1,1,1,3,3,3-hexamethyldisilazane (98%, ACROS), octyl acetate (99+%, Aldrich), *n*-butyllithium (2.5 M in hexanes, Aldrich), and 2,2,2-trifluoroethyl trifluoroacetate (99%, Aldrich) were used as received. Tetrabutylammonium perchlorate (TBAP, 98%, ACROS) was recrystallized twice prior to use. All solvents were obtained from typical commercial sources and were used without further treatment except for CH<sub>2</sub>Cl<sub>2</sub> which was freshly distilled prior to use. Water was supplied by a Barnstead Nanopure water system (18.3 M $\Omega$ ).

**Synthesis of Octyl Diazoacetate (ODA).** The ODA ligands were synthesized by following a modified literature procedure (Scheme 1).<sup>30</sup> Briefly, to a solution of 1,1,1,3,3,3-hexamethyldisilazane (1.3 mL, 6.4 mmol) in tetrahydrofuran (THF; 30 mL), cooled to 0 °C, was added *n*-butyllithium (2.6 mL, 6.4 mmol, 2.5 M in hexanes) dropwise over 20 min. The resultant solution was stirred at 0 °C for a further 30 min and then cooled to -78 °C. A solution of

## Scheme 1. Reaction Scheme of the Synthesis of the ODA Ligands



octyl acetate (1.0 g, 5.8 mmol) in THF (20 mL) was then added dropwise to the reaction mixture over 20 min and then stirred for 1 h at -78 °C. 2,2,2-Trifluoroethyl trifluoroacetate (0.9 mL, 7.0 mmol) was then added in one portion, and the reaction was stirred for a further 30 min and allowed to warm to ambient temperature. The reaction was quenched with dilute hydrochloric acid (1 M, 80 mL) and extracted with ether (3 × 40 mL). The combined organic extractions were then dried (Na<sub>2</sub>SO<sub>4</sub>) and concentrated under reduced pressure. The residue was then dissolved in acetonitrile (30 mL) to which was then added triethylamine (1.2 mL, 8.7 mmol), water (0.1 mL, 6.4 mmol) and a solution of methanesulfonyl azide (1.1 g, 8.7 mmol) in acetonitrile (20 mL), and the resultant mixture was stirred at ambient temperature for 16 h. The mixture was then diluted with ether (100 mL) and washed with aqueous sodium hydroxide (1 M; 3 × 60 mL), and the organic layer was dried (Na<sub>2</sub>SO<sub>4</sub>), filtered through a pad of silica, eluting with ether, and concentrated under reduced pressure to yield the title product as a yellow oil (1.1 g, 99%). The prepared ODA was characterized by Fourier transform infrared (FTIR) and <sup>1</sup>H NMR measurements. In the FTIR measurements in a KBr pellet, the characteristic vibrational bands of the diazo (N=N) and carbonyl (C=O) moieties were observed at 2111 and 1698 cm<sup>-1</sup>, respectively (vide infra). In <sup>1</sup>H NMR characterization, the spectral details (500 MHz; CDCl<sub>3</sub>) are as follows: 4.74 (1H, br s, CHN<sub>2</sub>), 4.16 (2H, t, *J* = 6.8, OCH<sub>2</sub>), 1.68–1.57 (2H, m, CH<sub>2</sub>), 1.38–1.27 (10H, m, 5 × CH<sub>2</sub>), 0.89 (3H, t, *J* = 7.0, CH<sub>3</sub>).

## Preparation of Ruthenium Nanoparticles Stabilized by ODA.

Ru nanoparticles were synthesized by reduction of ruthenium chloride in 1,2-propanediol according to the procedure described by Viau et al.<sup>31,32</sup> Briefly, 0.65 mmol of RuCl<sub>3</sub> and 2 mmol of NaAc were dissolved in 200 mL of 1,2-propanediol. The mixed solution was heated to 165 °C for 15 min under vigorous stirring. During the reaction, the color of the solution was found to change from red to pale green and finally to dark brown indicating the formation of Ru nanoparticles. After the colloid solution cooled to room temperature, ODA dissolved in toluene with threefold molar excess as compared to Ru was added into the solution under magnetic stirring overnight. An intense color appearance was observed in the toluene phase whereas the diol phase became colorless, signifying the extraction of the particles from the diol phase to the toluene phase. Such a phase transfer of Ru nanoparticles from the hydrophilic medium (diol) to the hydrophobic phase (toluene) indicated that the Ru particles were now capped with a hydrophobic surfactant layer, most likely arising from the strong affinity of the diazo moieties to the ruthenium surface forming Ru=C carbene bonds (further confirmation by <sup>1</sup>H NMR and FTIR measurements, vide infra). With the addition of 20 mL of Nanopure water to further separate the two phases, the toluene portion was collected and dried at reduced pressure. Copious methanol was then used to remove excessive ligands, affording purified Ru nanoparticles. Like alkanethiolate-protected gold nanoparticles, the resulting Ru nanoparticles (denoted as Ru=C8) were found to be soluble in apolar solvents, such as dichloromethane (DCM) and hexane, but not in polar solvents, such as alcohols and water.

(24) Zamborini, F. P.; Gross, S. M.; Murray, R. W. *Langmuir* **2001**, *17*, 481–488.

(25) Tong, M. C.; Chen, W.; Sun, J.; Ghosh, D.; Chen, S. W. *J. Phys. Chem. B* **2006**, in press.

(26) Chen, S. W.; Murray, R. W.; Feldberg, S. W. *J. Phys. Chem. B* **1998**, *102*, 9898–9907.

(27) Tulevski, G. S.; Myers, M. B.; Hybertsen, M. S.; Steigerwald, M. L.; Nuckolls, C. *Science* **2005**, *309*, 591–594.

(28) Dinh, H. N.; Ren, X. M.; Garzon, F. H.; Zelenay, P.; Gottesfeld, S. *J. Electroanal. Chem.* **2000**, *491*, 222–233.

(29) Nashner, M. S.; Frenkel, A. I.; Somerville, D.; Hills, C. W.; Shapley, J. R.; Nuzzo, R. G. *J. Am. Chem. Soc.* **1998**, *120*, 8093–8101.

(30) Danheiser, R. L.; Miller, R. F.; Brisbois, R. G.; Park, S. Z. *J. Org. Chem.* **1990**, *55*, 1959–1964.

(31) Viau, G.; Brayner, R.; Poul, L.; Chakroune, N.; Lacaze, E.; Fievet-Vincent, F.; Fievet, F. *Chem. Mater.* **2003**, *15*, 486–494.

(32) Chakroune, N.; Viau, G.; Ammar, S.; Poul, L.; Veautier, D.; Chehimi, M. M.; Mangeney, C.; Villain, F.; Fievet, F. *Langmuir* **2005**, *21*, 6788–6796.

**Transmission Electron Microscopy.** The particle core diameter was measured with a JEOL 1200 EX transmission electron microscope (TEM) at 80 keV. The samples were prepared by casting a drop of the particle solution (~1 mg/mL) in DCM onto a 200-mesh carbon-coated copper grid. The particle core diameter was estimated by using ImageJ analysis of the TEM micrographs.

**Metathesis-Based Ligand Exchange Reaction.** As an illustrating example, the Ru=C8 particles obtained above were then subject to ligand exchange reactions with 11-bromo-1-undecene. In a typical reaction, Ru=C8 and 11-bromo-1-undecene (the molar ratio of 11-bromo-1-undecene to particle-bound carbene ligands was 6:1) were dissolved in DCM under magnetic stirring. At different reaction times (from 2 to 35 h), an aliquot of the solution was taken out and the particles were precipitated by the addition of excessive ethanol. The nanoparticles were separated by centrifugation and washed by copious ethanol to remove the excessive 11-bromo-1-undecene and displaced ligands. Finally the dried particles (denoted as Ru=C10Br) were dissolved in CDCl<sub>3</sub> and characterized by <sup>1</sup>H NMR spectroscopy.

**Spectroscopies.** UV–vis spectroscopic studies were performed with an ATI Unicam UV4 spectrometer using a 1-cm quartz cuvette with a resolution of 2 nm. The purity of the particles and the dynamics of the ligand exchange reaction were examined by using proton NMR spectroscopy (Varian Unity 500 MHz) with a concentrated solution of particles dissolved in CDCl<sub>3</sub>. FTIR measurements were carried out with a Perkin-Elmer FTIR spectrometer (Spectrum One) where the samples were prepared by compressing the materials of interest into a KBr pellet. The spectral resolution was 4 cm<sup>-1</sup>.

**Electrochemistry.** Voltammetric measurements were carried out with a CHI 440 electrochemical workstation. A polycrystalline gold disk electrode (sealed in a glass tubing) was used as the working electrode. A Ag/AgCl wire and a Pt coil were used as the (quasi)-reference and counter electrodes, respectively. The gold electrode was first polished with alumina slurries of 0.05 μm and then cleansed by sonication in 0.1 M HNO<sub>3</sub>, H<sub>2</sub>SO<sub>4</sub> and Nanopure water successively. Prior to data collection, the electrolyte solution was deaerated by bubbling ultrahigh-purity N<sub>2</sub> for at least 20 min and blanketed with a nitrogen atmosphere during the entire experimental procedure.

## Results and Discussion

### Quantized Charging of Ruthenium Nanoparticles.

Figure 1 shows the cyclic voltammetry (CV) and differential pulse voltammetry (DPV) of the Ru=C8 particles in DCM containing 0.1 M TBAP as the supporting electrolyte. In the CV measurements, several weak voltammetric peaks can be observed within the potential range of -1.0 to +0.8 V (vs Ag/AgCl). These features are much better-resolved in DPV measurements, where there are at least four pairs of well-defined voltammetric peaks with magnitudes well above the background noise level. These are ascribed to the quantized capacitance charging of the Ru nanoparticles. Their formal potentials (Table 1) can be determined at -0.68, -0.41, -0.092, and 0.44 V, respectively. From the average potential spacing ( $\Delta V$ ) between adjacent quantized charging peaks (~0.37 V), the molecular capacitance ( $C_{MPC}$ ) of the Ru nanoparticles can be evaluated ( $C_{MPC} = e/\Delta V$  with  $e$  being the electronic charge) at about 0.43 aF. In addition, the small peak splittings ( $\Delta E_p \leq 20$  mV) suggest very facile electron-transfer processes, and the faradic reactions behave reversibly, akin to those with other metal nanoparticles.<sup>20–22</sup>

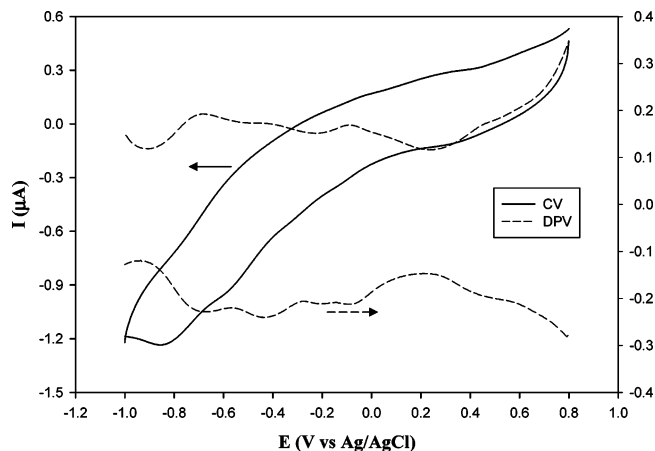


**Figure 1.** CV and DPV voltammograms of Ru=C8 nanoparticles at a concentration of 4.7 mg/mL in DCM with 0.1 M TBAP. The gold disk electrode area is 0.9 mm<sup>2</sup>. In CV, the potential scan rate is 100 mV/s; and in DPV, the dc ramp is 4 mV/s, pulse amplitude is 50 mV, and pulse width is 200 ms. Note that the y-axis scales are different for the CV and DPV measurements.

**Table 1.** Peak Potentials of Quantized Charging of Ru=C8 Nanoparticles

peak no.	$E_{p,a}^a$ (V)	$E_{p,c}^a$ (V)	$E^o$ (V)	$\Delta E_p$ (V)
1	+0.448	+0.432	+0.440	0.016
2	-0.092	-0.092	-0.092	0.000
3	-0.404	-0.424	-0.414	0.020
4	-0.684	-0.676	-0.680	0.008

<sup>a</sup> Subscripts (a and c) denote anodic and cathodic peaks, respectively. All potentials are referenced to the Ag/AgCl reference, and data are collected from the DPV measurements in Figure 1.

The above results represent a novel observation of electrochemical quantized charging with nanoparticles beyond the coinage metals.<sup>20–22</sup> As mentioned earlier, most quantized charging phenomena are limited to gold particles<sup>20</sup> with a few reports with Cu,<sup>21</sup> Pd,<sup>22–24</sup> and Ag<sup>25</sup> nanoparticles. It should be noted that to observe these single electron transfer (SET) events, the energetic barrier for SET ( $e^2/C_{MPC}$ ) must exceed the thermal kinetic energy ( $k_B T$  with  $k_B$  being the Boltzmann constant). As the capacitance for a monolayer-protected nanoparticle is  $C_{MPC} = 4\epsilon\epsilon_0(r/d)(r + d)$ , where  $\epsilon$  is the dielectric constant of the protecting layer,  $\epsilon_0$  is the permittivity,  $r$  is the core radius, and  $d$  is the monolayer thickness, the particle dimensions must be confined within the nanometer range to effect the quantized charging features at ambient temperature. For instance, the core diameter of the Ru=C8 particles used in the above voltammetric measurements can be estimated to be approximately 1.6 nm from the molecular capacitance (0.43 aF) by assuming  $\epsilon = 3$  and  $d$  is equal to the fully extended chain length of the protecting ligand, which is 1.24 nm as calculated by Hyperchem.<sup>26</sup> Note that the particle core size estimated here is rather consistent with that from TEM measurements, as shown in Figure 2. First, it can be seen that the particles are very well disperse with no apparent aggregates, suggesting effective passivation of the carbene ligands on the Ru particle surface (vide infra). In addition, from the particle core size histogram (Figure 2, inset), one can see that the overall average core diameter is  $2.12 \pm 0.72$  nm, with approximately 40% in the narrow range of 1.2–2.4 nm. It should be noted that, in electrochemical measurements, the contributions to the quantized charging currents primarily arise from particles

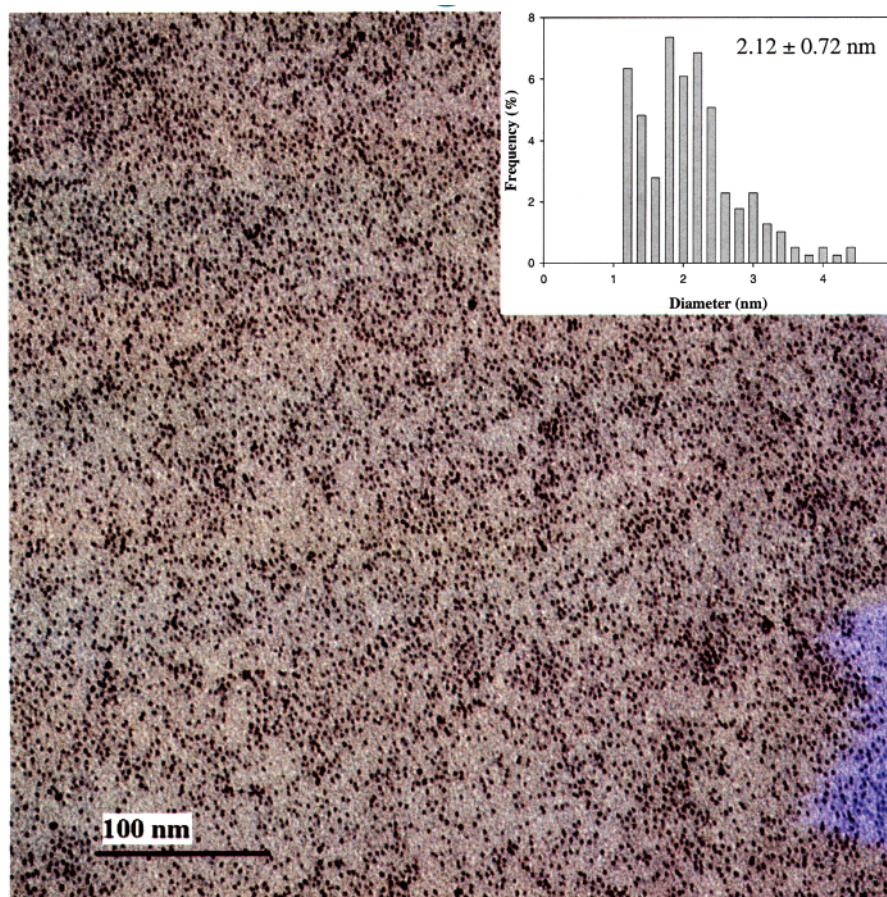


**Figure 2.** Representative TEM micrograph of the Ru=C8 particles. The inset shows the particle core size histogram, and the overall average is shown as the figure legend. The scale bar is 100 nm.

with a core diameter smaller than 2.5 nm,<sup>26</sup> whereas larger particles generally contribute to the baseline currents. Thus, the core diameter estimated from the quantized charging mainly reflects those that are in the lower end of the histogram, whereas in TEM measurements, it is the ensemble statistic average of all particles in the image.

In addition, the metal core must be chemically stable. For instance, for freshly prepared Cu particles protected by an alkanethiolate monolayer,<sup>21</sup> the quantized charging features are very well-defined, whereas after prolonged exposure to the ambient atmosphere, the formation of an oxide layer renders that the particles behave like a semiconductor material, hence, the diminishment of the voltammetric features. In fact, synthesis of nanometer-sized particles and chemical inertness of core metals are two of the major challenges for group V and lighter transition metals. By contrast, gold nanoparticles exhibit long-term chemical stability, and the synthetic procedure for particles with a diameter in the range of 1–5 nm has been quite well-documented.<sup>33</sup> In the current study with Ru nanoparticles, the particles are found to be stable in air. We observed no significant variation of the particle optical and electrochemical properties even after exposure to the ambient atmosphere for 1 month. Bulk ruthenium metal has been known to be

inert to oxidation in air.<sup>34</sup> In addition, the fact that we observed very clear quantized charging responses even with as-prepared particles (i.e., without any postsynthesis fractionation) strongly suggests that the particles were very monodisperse, consistent with the TEM measurements.

Furthermore, on the basis of the voltammetric results in Figure 1 and the TEM data in Figure 2, some insights into the nanoparticle structure can be obtained. First, the interactions between the freshly prepared ruthenium nanoparticles and the diazo ligands must be sufficiently strong to withstand extensive rinsing and repetitive dispersion, most probably by the formation of Ru=C double bonds. Recently it was reported<sup>27</sup> that diazomethane reacted with freshly prepared ruthenium metal films to form Ru=C  $\pi$  bonding linkages. In this reaction, the C=N<sub>2</sub> bond in the diazo ligands cleaves, and the resulting =CHCOO(CH<sub>2</sub>)<sub>7</sub>CH<sub>3</sub> carbene fragment binds to the ruthenium surface directly. As far as we know, the approach presented here represents the first attempt of using such covalent linkages to stabilize transition-metal nanoparticles (Tulevski et al.<sup>27</sup> also mentioned that Ru nanoparticles were used, but no details were given in their study). Second, the appearance of well-defined quantized charging peaks in electrochemical measurements and the submicrofarad particle capacitance provide further supporting evidence that the Ru core surface must be coated with a low-dielectric layer.

(33) Hostetler, M. J.; Wingate, J. E.; Zhong, C. J.; Harris, J. E.; Vachet, R. W.; Clark, M. R.; Londono, J. D.; Green, S. J.; Stokes, J. J.; Wignall, G. D.; Glish, G. L.; Porter, M. D.; Evans, N. D.; Murray, R. W. *Langmuir* **1998**, *14*, 17–30.

(34) Lide, D. R. *Handbook of Chemistry and Physics*, 76th ed.; CRC: Boca Raton, 1995.

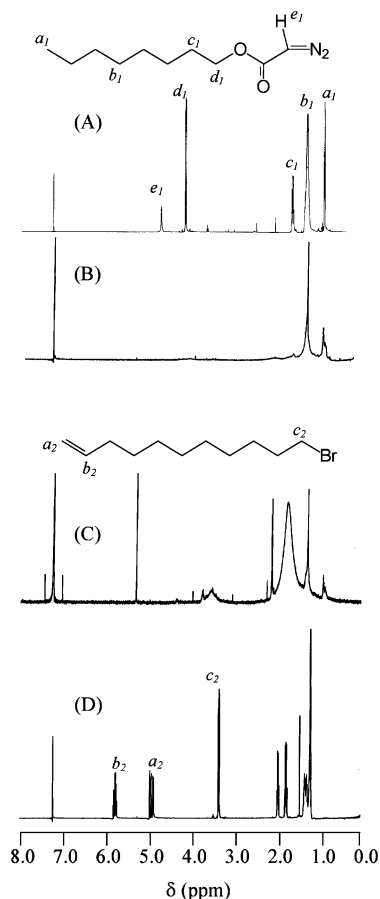
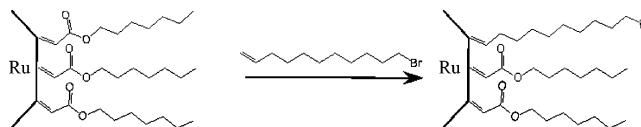


**Figure 3.**  $^1\text{H}$  NMR spectra of the Ru=C8 particles during exchange reactions with 11-bromo-1-undecene ligands in DCM: (A) free ODA ligands; (B) Ru=C8 particles; (C) Ru=C8 particles mixed with 11-bromo-1-undecene after 35 h of reaction; and (D) free 11-bromo-1-undecene. The molar feed ratio of the particle-bound carbene ligands vs 11-bromo-1-undecene was 1:6, and the concentration of 11-bromo-1-undecene was 3.3 mM.

**Metathesis-Based Ligand Exchange Reactions.** Ruthenium-carbene complexes have long been used as effective catalysts in metathesis reactions for organic syntheses.<sup>35</sup> Recently it was shown<sup>27</sup> that metathesis reactions can also occur on freshly prepared ruthenium metal thin film surfaces with a carbene adlayer. Such unique properties provide a fundamental platform for the functionalization of carbene-functionalized Ru nanoparticles where the metathesis reaction is extended to the three-dimensional structures. In addition, by taking advantage of the solubility characteristics of the particles, one can monitor the exchange reaction by using a variety of analytical techniques that are not accessible to the two-dimensional counterparts, as demonstrated extensively in alkanethiolate-protected gold (AuSR) particles.<sup>14–18</sup> In the present study, NMR spectroscopy is the tool of choice to monitor the exchange dynamics of ruthenium particles.

Figure 3 depicts the  $^1\text{H}$  NMR spectra of the (A) free ODA molecules and (B) the Ru=C8 particles. As observed previously with AuSR nanoparticles,<sup>33,36</sup> substantial broadening of the NMR spectral features occurred when the ligands

**Scheme 2.** Metathesis-Based Exchange Reaction of Carbene-Functionalized Ruthenium Nanoparticles



were bound onto the nanoparticle surface. By comparing panels A and B, one can see that the broadening is more significant for the protons that reside near the metal core than those close to the periphery. Consequently, only the protons from the terminal methyl group and the nearby methylene moieties (namely, the  $a_1$  and  $b_1$  protons) can be resolved whereas those close to the particle core surface (i.e., the  $c_1$ ,  $d_1$ , and  $e_1$  protons) become broadened into the baseline. Several factors have been proposed to account for this observation<sup>33</sup>: (i) Because of the curvature of the particle core, the packing of the protecting ligands becomes increasingly dense from the particle peripheral to the core surface. The solid-like structure at the ligand/core interface leads to rapid spin relaxation from dipolar interactions. (ii) Structural heterogeneity on the particle core surface (vertices, edges, and terraces) will cause a distribution of the chemical shifts. (iii) Particle core size dispersity will lead to the variation of the tumbling rate of the particle molecules in solution which can also contribute to the spin-spin relaxation ( $T_2$ ) broadening.

Upon the introduction of 11-bromo-1-undecene into the Ru=C8 particle solution, the NMR spectra exhibit a dynamic variation as a result of the metathesis-based exchange reaction on the particle surface (Scheme 2). The molar ratio of the added 11-bromo-1-undecene (3.3 mM) is 6:1 in relation to the moles of the carbene ligands on the Ru particles. Figure 3C depicts a representative spectrum which was acquired after 35 h of reaction. It should be noted that the particles underwent extensive rinsing to remove excessive and free ligands prior to the spectral collection. The spectral features are again broadened, as observed earlier. In comparison to the spectrum of the 11-bromo-1-undecene ligands (panel D), the new and broad peak that emerges at approximately  $\delta = 3.6$  ppm can be ascribed to the  $\alpha$ -methylene protons next to the terminal Br moiety ( $c_2$ ), signifying the successful incorporation of the bromide ligands onto the particle surface by surface metathesis reaction. The disappearance of the  $a_2$  and  $b_2$  peaks is also consistent with the cleavage of the C=C double bond in the 11-bromo-1-undecene molecule, the formation of the new Ru=C bond, and hence the resulting broadening of the carbene proton. The appearance of the methyl protons at  $\delta = 0.9$  ppm ( $a_1$ ) indicates that at this point (35 h), not all the original carbene ligands are replaced by metathesis reactions with 11-bromo-1-undecene molecules. In fact, from the ratio of the peak areas from these two kinds of protons, the exchange extent can be estimated to be 90%, namely, at 35 h, 90% of the original protecting ligands undergo metathesis reactions with the 11-bromo-1-undecene molecules.

The overall exchange dynamics is depicted in Figure 4, where the symbols are the experimental data collected from Figure 3 and the line is the corresponding exponential fitting. First, within the current experimental context, the maximum

(35) Trnka, T. M.; Grubbs, R. H. *Acc. Chem. Res.* **2001**, *34*, 18–29.

(36) Terrill, R. H.; Postlethwaite, T. A.; Chen, C. H.; Poon, C. D.; Terzis, A.; Chen, A. D.; Hutchison, J. E.; Clark, M. R.; Wignall, G.; Londono, J. D.; Superfine, R.; Falvo, M.; Johnson, C. S.; Samulski, E. T.; Murray, R. W. *J. Am. Chem. Soc.* **1995**, *117*, 12537–12548.

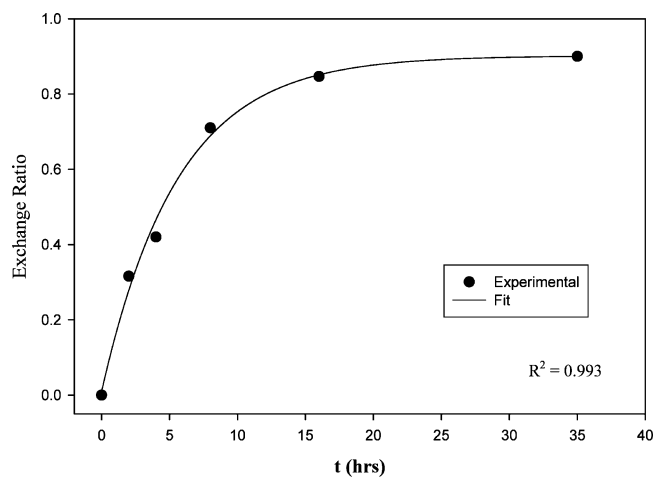


**Figure 4.** Reaction dynamics of the particle exchange reaction. Symbols are experimental data collected from the NMR spectra in Figure 3C, whereas the line represents the exponential fitting by the equation  $y = y_0 + ae^{-bt}$ . The fitting parameters are  $y_0 = 0.902$ ,  $a = -0.893$ , and  $b = 0.179$ .

exchange extent is 90% which can be achieved after 35 h of reaction. For comparison, at 4 h, about 42% of the original carbene ligands have undergone metathesis reactions with 11-bromo-1-undecene. Second, as the 11-bromo-1-undecene ligand is in large excess as compared to the concentration of the Ru=C8 particles, from the fitting of the experimental data, the pseudo-first-order reaction rate constant can be estimated at  $0.179 \text{ h}^{-1}$ . Taking into account the concentration of 11-bromo-1-undecene ( $3.3 \text{ mM}$ ), one can then evaluate the corresponding second-order rate constant to be  $1.5 \times 10^{-2} \text{ M}^{-1} \text{ s}^{-1}$ , which is about twice as much as that<sup>37</sup> observed with AuSR particles in the exchange reaction with another thiol ligand. The above observation demonstrates the proof of concept that the metathesis reaction may be exploited for the chemical functionalization of Ru nanoparticles. Furthermore, potentially the obtained Ru particles with terminal bromide groups can be used for further chemical decoration by coupling reactions through the labile Br moieties.<sup>38</sup>

**Spectroscopies.** Nanosized metal particles exhibit unique optical characteristics with an exponential decay of the absorption profile with increasing wavelength, the so-called Mie scattering.<sup>39</sup> Figure 5 shows the UV-vis absorption spectra of the ruthenium particles before and after exchange reactions. It can be seen that overall, the profiles are very similar, both consistent with the Mie characteristics. Nonetheless, there is a small discrepancy where the absorption spectrum becomes slightly less steep after exchange reaction (Ru=C10Br, dotted line) than of the original particles (Ru=C8, solid line). This may be attributable to the slight variation of the particle solubility properties as a consequence of the change of the packing density of the protecting ligands on the particle surface before and after exchange reaction. For comparison, the Ru complex precursor (RuCl<sub>3</sub>, dashed line) exhibits a totally different absorption profile with two broad

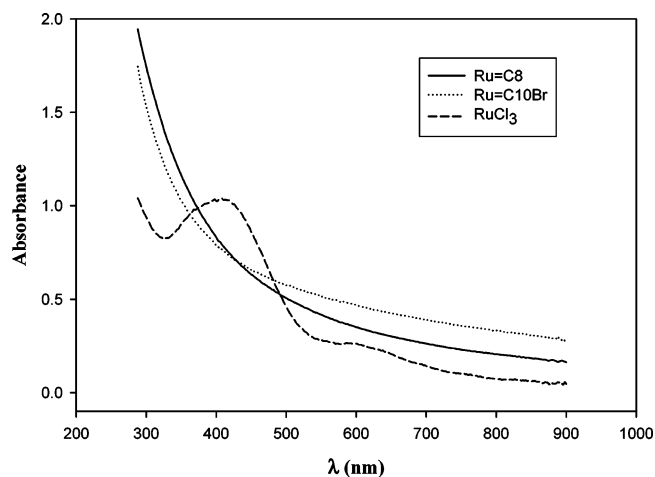


**Figure 5.** UV-vis spectra of the Ru particles before (Ru=C8) and after (Ru=C10Br, same as that in Figure 3C) exchange reactions. Particle concentrations are both  $0.1 \text{ mg/mL}$  in DCM. For the precursor RuCl<sub>3</sub>, the concentration was  $3.3 \text{ mM}$  in water.

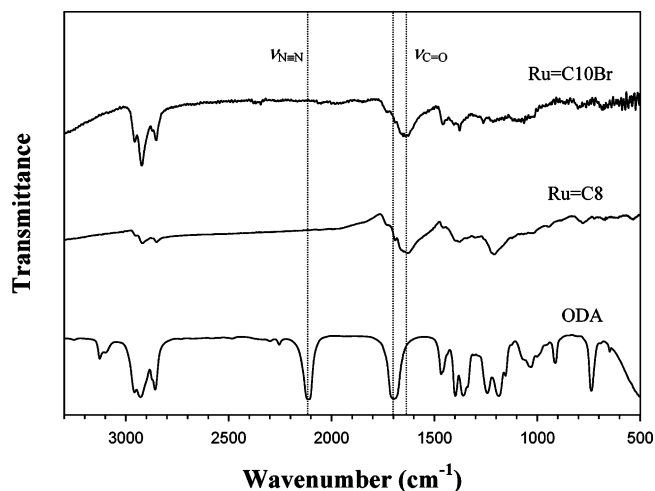


**Figure 6.** FTIR spectra of the ODA molecules and ruthenium particles before (Ru=C8) and after (Ru=C10Br, same as that in Figure 3C) surface exchange reactions.

peaks at about 420 and 600 nm which may be ascribed to the metal–ligand (M–L) transitions.

In FTIR measurements (Figure 6), free ODA ligands exhibit the characteristic vibrational bands at  $2111$  and  $1698 \text{ cm}^{-1}$  for the diazo ( $\text{N}\equiv\text{N}$ ) and carbonyl ( $\text{C}=\text{O}$ ) moieties, respectively. With the cleavage of the  $\text{C}=\text{N}_2$  bond and the resulting carbene fragment binding to the Ru surface, the diazo band disappears. Concurrently, the carbonyl stretching band shifts downward to  $1640 \text{ cm}^{-1}$  (which can be seen in both the Ru=C8 and the Ru=C10Br particles, Figure 6, and is consistent with the singlet state of the metal–carbene double bond).<sup>40</sup> Such a red shift has also been observed in metal–carbene complexes,<sup>40</sup> which was ascribed to the delocalization of the radical on the  $\text{C}_{\text{carbene}}$  over the  $\alpha$ -carbonyl group.

### Concluding Remarks

Stable ruthenium nanoparticles were synthesized by taking advantage of the strong affinity of diazo moieties for freshly

(37) Song, Y.; Murray, R. W. *J. Am. Chem. Soc.* **2002**, *124*, 7096–7102.  
(38) Templeton, A. C.; Hostetler, M. J.; Warmoth, E. K.; Chen, S. W.; Hartshorn, C. M.; Krishnamurthy, V. M.; Forbes, M. D. E.; Murray, R. W. *J. Am. Chem. Soc.* **1998**, *120*, 4845–4849.

(39) Creighton, J. A.; Eadon, D. G. *J. Chem. Soc., Faraday Trans.* **1991**, *87*, 3881–3891.

(40) Iwakura, I.; Tanaka, H.; Ikeno, T.; Yamada, T. *Chem. Lett.* **2004**, *33*, 140–141.

prepared ruthenium metal surfaces through the formation of a Ru=C  $\pi$  bond, as manifested in spectroscopic measurements. Because of the monodisperse nanometer core size, the resulting particles exhibited molecular capacitor characteristics which were manifested in electrochemical quantized capacitance charging measurements. In addition, the unique properties of metathesis reactions on ruthenium surfaces were exploited to initiate surface place exchange reactions on these ruthenium particles with other vinyl derivatives, leading to ready manipulation of the particle chemical/physical properties through surface functionalization. The reaction dynamics was monitored by  $^1\text{H}$  NMR spectroscopic measurements, and the exchange rate constant was found to be substantially faster than that of alkanethiolate-protected gold particles with another thiol.

Comparative studies with thiol derivatives are currently underway, and the results will be reported in due course.

In a recent paper,<sup>41</sup> Schiffrin and co-workers reported the synthesis of gold and platinum nanoparticles stabilized by metal-carbon bonds after reduction of diazonium derivatives of the capping ligands.

**Acknowledgment.** This work was supported in part by a CAREER Award from the National Science Foundation (CHE-0456130), the Petroleum Research Fund administered by the American Chemical Society (39729-AC5M), and the University of California—Santa Cruz.

CM061595L

---

(41) Mirkhalaf, F.; Paprotny, J.; Schiffrin, D. J. *J. Am. Chem. Soc.* **2006**, *128*, 7400–7401.